J. Fluid Mech. (1995), *vol.* 300, *pp.* 207–229

Mixed-convection laminar film condensation on a semi-infinite vertical plate

By JIAN-JUN SHU† AND GRAHAM WILKS
Department of Mathematics, University of Keele, Keele, Staffordshire ST5 5BG, UK

(Received 19 July 1994 and in revised form 16 May 1995)

The flow of a uniform stream of pure saturated vapour past a cold, semi-infinite vertical plate is examined. The formulation incorporates the limits of both pure forced-convection and pure body-force-convection laminar film condensation. Detailed asymptotic and exact numerical solutions are obtained and comparisons drawn with approximate methods and experimental results reported in the literature.

1. Introduction

Since the pioneering work of Nusselt (1916) on laminar film condensation in quiescent ambient surroundings the original model has been progressively refined to incorporate thermal convection (Rohsenow 1956), inertial effects (Sparrow & Gregg 1959) and vapour shear (Koh, Sparrow & Hartnett 1961). The work of Sparrow & Gregg was especially noteworthy as it introduced the mathematical techniques of boundary layer theory into the subject and identified similarity solutions of the governing equations when convective inertia terms were included. The theme of similarity solution has been central to a number of further developments particularly in examinations of forced-convection laminar film condensation resulting from the flow of saturated vapour over sub-cooled surfaces. These include Cess (1960), Koh (1962) and Chung (1961). The most comprehensive analytic investigation of such forced convection condensation is that of Beckett & Poots (1972). Exploiting boundary layer perturbation techniques they examine non-similar flow configurations which include non-uniform velocity distributions of the saturated vapour. In particular they investigate the results of adverse pressure gradients in the main stream of flowing vapour and indicate the lubricating effect of the condensate film. The delayed separation of the boundary layer system is demonstrated by pursuing an exact numerical solution of the coupled equations governing the simultaneous flow of vapour and condensate using methods based on Hartree & Womersley (1937) and Terrill (1960). In an attempt to obviate the difficulties of a full numerical solution for strongly non-similar configurations Beckett & Poots present useful approximate solutions based on 'thin' and 'thick' film asymptotic analysis of the governing equations. Their work is central to the work that follows. Here we examine the alternative non-similar configuration of combined or mixed forced and body-force convection laminar film condensation flow along a semi-infinite plate. However, although the underlying flow is non-similar overall, in the limits of pure forced convection or pure body-force convection similarity solutions do apply. Thus, as opposed to the flows

† Present address: Department of Applied Mathematical Studies, University of Leeds, Leeds LS2 9JT, UK.

to breakdown of Beckett & Poots the mixed-convection condensation problem is a progression between known similarity states. As a consequence perturbation schemes can be examined in detail about each limiting similarity state. The 'thin' and 'thick' film scalings of Beckett & Poots are found to be especially instructive. In conjunction with the perturbation analyses, for the first time, a comprehensive numerical solution has also been obtained. An adaptation of the Keller box method has been developed which takes advantage of the known similarity extremes. For single-phase flows Hunt & Wilks (1981) have described an appropriate methodology which has subsequently been used successfully in a wide variety of boundary layer settings both in that form and in a variant presented by Raju, Liu & Law (1984). The adaptation, whilst accommodating the overall non-similarity, must necessarily be adjusted to incorporate the new features of finite film thickness and multiphase. The scheme is both accurate and robust. The exact solutions may not only be compared with the present perturbation schemes but also with earlier integral treatments of the problem by Jacobs (1966) and Fujii & Uehara (1972). Specific comparison is also made with the experimental results reported by Jacobs (1965).

2. The problem and governing equations

The problem under examination is illustrated in figure 1. A uniform stream of pure saturated vapour flows downwards past the leading edge of a semi-infinite vertical plate. The constant free-stream velocity is aligned parallel to the local gravity field and is designated U_∞ and the temperature of the vapour is denoted T^*. As a result of maintaining the temperature of the plate at $T_w < T^*$ a condensate film will develop at the plate surface. The accumulating condensate will respond to the local gravity field and a downward film flow will be generated. At the film surface an adjustment between the local velocity of the free surface and that of the uniform stream of vapour induces an accompanying vapour boundary layer. The aim is to establish full details of velocity and temperature distributions within the condensate film and the vapour shear layer at all stations along the plate from the leading edge. The flow and heat transfer characteristics of skin friction coefficient, heat transfer coefficient and condensate film thickness can then be evaluated.

The flow is assumed to be steady and two-dimensional and the condensate and vapour are taken as incompressible fluids. The coordinate system is Cartesian (x, y) where the plate coincides with the x-axis and y measures distances normal to the plate. (u,v) are the velocity components of the condensate associated with increasing x and y respectively. The temperature of the condensate is denoted by T and the interface separating the condensate and vapour phases is designated $y = \delta(x)$, i.e. the condensate film thickness.

A set of intrinsic coordinates attached to the interface describe the vapour phase: x^* measures distance along the interface and y^* the distance normal to it. Velocity components in the directions of increasing x^*, y^* are u^*, v^* respectively. The starred notation will be used throughout to identify quantities associated with the vapour flow.

It is further assumed that the thickness of the condensate is small compared with a typical dimension of the surface and thus $x = x^*$. The boundary layer approximation is also invoked which assumes that all changes in physical quantities normal to the condensate/vapour interface are large compared with changes in the x-direction. Finally the model assumes that the condensate free surface is constantly in contact with pure, saturated vapour at temperature T^*. The governing equations will

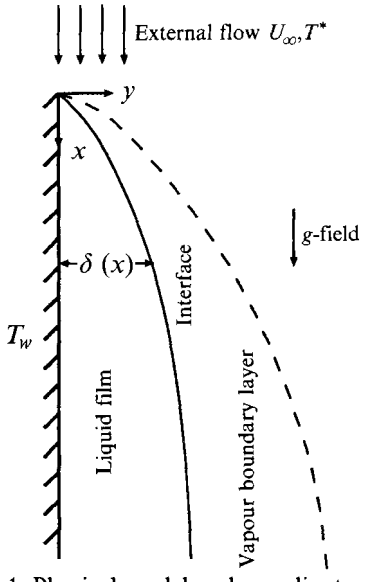

FIGURE 1. Physical model and coordinate system.

accordingly represent conservation of mass, momentum and energy for the condensate film and conservation of mass and momentum in the vapour phase. These are:

condensate $x \geqslant 0, 0 \leqslant y \leqslant \delta(x)$

$$\frac{\partial u}{\partial x} + \frac{\partial v}{\partial y} = 0, \tag{2.1}$$

$$\rho u \frac{\partial u}{\partial x} + \rho v \frac{\partial u}{\partial y} = g(\rho - \rho^*) + \mu \frac{\partial^2 u}{\partial y^2}, \tag{2.2}$$

$$\rho C_p (u \frac{\partial T}{\partial x} + v \frac{\partial T}{\partial y}) = k \frac{\partial^2 T}{\partial y^2}; \tag{2.3}$$

vapour $x^* \geqslant 0, y^* = y - \delta(x) \geqslant 0$

$$\frac{\partial u^*}{\partial x} + \frac{\partial v^*}{\partial y^*} = 0, \tag{2.4}$$

$$\rho^* u^* \frac{\partial u^*}{\partial x} + \rho^* v^* \frac{\partial u^*}{\partial y^*} = \mu^* \frac{\partial^2 u^*}{\partial y^{*2}}. \tag{2.5}$$

(Temperature $= T^*$ throughout.)

The boundary conditions under which equations (2.1)–(2.5) are to be solved are:
(*a*) the no slip, impermeability and temperature conditions at the plate

$$u = v = 0, \quad T = T_w \qquad x \geqslant 0, y = 0; \tag{2.6}$$

(*b*) the temperature and continuity conditions at the interface $x \geqslant 0, y^* = y - \delta(x) = 0$
(i) temperature:

$$T = T^*, \tag{2.7}$$

(ii) mass flow:

$$\rho^* \left(v^* - u^* \frac{\mathrm{d}\delta}{\mathrm{d}x} \right) = \rho \left(v - u \frac{\mathrm{d}\delta}{\mathrm{d}x} \right) = -\frac{\mathrm{d}}{\mathrm{d}x} \left(\int_0^{\delta(x)} \rho u \mathrm{d}y \right), \tag{2.8}$$

(iii) tangential velocity:

$$u^* = u, \tag{2.9}$$

(iv) shear stress:

$$\mu^* \frac{\partial u^*}{\partial y^*} = \mu \frac{\partial u}{\partial y}, \tag{2.10}$$

(and neglecting curvature $p^* = p$);

(*c*) the velocity condition away from the plate

$$u^* \to U_\infty, \qquad x \geqslant 0, y^* \to \infty; \tag{2.11}$$

(*d*) the overall energy balance, including sub-cooling within the condensate layer as well as the release of latent heat at the interface, given by

$$-\int_0^x k \left(\frac{\partial T}{\partial y} \right)_{y=0} \mathrm{d}x + \int_0^{\delta(x)} \rho u h_{fg} \mathrm{d}y + \int_0^{\delta(x)} \rho u C_p (T^* - T) \mathrm{d}y = 0. \tag{2.12}$$

Here $\rho, \mu, C_p, k, h_{fg}, p$ and $\nu = \mu/\rho$ denote density, dynamic viscosity, specific heat, thermal conductivity, latent heat, pressure and kinematic viscosity respectively. An asterisk signifies a vapour quantity. The temperature differential $\Delta T = T^* - T_w$ is considered such as to allow all physical properties to be approximated as constant. Hence (2.1) and (2.4) appear as incompressible continuity equations.

The significant non-dimensional parameters in the problem are the Reynolds number, Froude number and Prandtl number defined respectively by

$$Re_x = \frac{U_\infty x}{\nu}, \quad Fr_x = \frac{U_\infty^2}{gx}, \quad P_r = \frac{C_p \mu}{k}. \tag{2.13}$$

Although the semi-infinite geometry lacks a characteristic length scale the local relative importance of inertia and gravity defines a characteristic length scale

$$\xi = \frac{gx}{U_\infty^2} \left(= \frac{1}{Fr_x} \right). \tag{2.14}$$

This non-dimensional coordinate provides a unified framework within which the features of dominant forced convection condensation and dominant body force convection condensation may be associated with small and large ξ respectively. It underpins the numerical algorithm which establishes comprehensive solutions for the flow at all stations along the plate $0 < \xi < \infty$.

3. The solutions near the leading edge

Near the leading edge of the plate the flow will predominantly be forced-convection laminar film condensation with similarity features as identified by Cess (1960). The influence of gravity will appear as a perturbation about the associated similarity solution. The appropriate transformations which exploit this appraisal of the flow and allow examination of the gravitational perturbation effects and which simultaneously

normalise the condensate film thickness are

$$\psi = \lambda(2\nu U_\infty x)^{1/2} F(\xi, \phi), \quad \phi = \eta/\eta_\delta(\xi) = \frac{\lambda}{\eta_\delta(\xi)} \frac{U_\infty^{1/2}}{(2\nu)^{1/2}} \frac{y}{x^{1/2}}, \tag{3.1}$$

$$\psi^* = (2\nu^* U_\infty x)^{1/2} f^*(\xi, \eta^*), \quad \eta^* = \frac{U_\infty^{1/2}}{(2\nu^*)^{1/2}} \frac{y^*}{x^{1/2}}, \tag{3.2}$$

$$T - T^* = (T_w - T^*)\Theta(\xi, \phi), \tag{3.3}$$

where $\lambda = ((\rho - \rho^*)/\rho)^{1/4}$ and $\eta_\delta(\xi)$ is the value of η at $y = \delta(x)$.

The boundary layer equations (2.1)–(2.5) and the boundary conditions (2.6)–(2.11) transform, respectively, to the following system of equations:

$$\frac{\partial^3 F}{\partial \phi^3} + \eta_\delta(\xi) F \frac{\partial^2 F}{\partial \phi^2} + 2\xi \eta_\delta^3(\xi) = 2\xi \left[\eta_\delta(\xi) \frac{\partial F}{\partial \phi} \frac{\partial^2 F}{\partial \xi \partial \phi} - \frac{\mathrm{d}\eta_\delta(\xi)}{\mathrm{d}\xi} \left(\frac{\partial F}{\partial \phi} \right)^2 - \eta_\delta(\xi) \frac{\partial^2 F}{\partial \phi^2} \frac{\partial F}{\partial \xi} \right], \quad 0 < \phi < 1, \tag{3.4}$$

$$\frac{1}{P_r} \frac{\partial^2 \Theta}{\partial \phi^2} + \eta_\delta(\xi) F \frac{\partial \Theta}{\partial \phi} = 2\xi \eta_\delta(\xi) \left[\frac{\partial F}{\partial \phi} \frac{\partial \Theta}{\partial \xi} - \frac{\partial \Theta}{\partial \phi} \frac{\partial F}{\partial \xi} \right], \quad 0 < \phi < 1, \tag{3.5}$$

$$\frac{\partial^3 f^*}{\partial \eta^{*3}} + f^* \frac{\partial^2 f^*}{\partial \eta^{*2}} = 2\xi \left(\frac{\partial f^*}{\partial \eta^*} \frac{\partial^2 f^*}{\partial \xi \partial \eta^*} - \frac{\partial^2 f^*}{\partial \eta^{*2}} \frac{\partial f^*}{\partial \xi} \right), \quad \eta^* > 0, \tag{3.6}$$

with boundary conditions

$$F(\xi, 0) = 0, \quad \frac{\partial F(\xi, 0)}{\partial \phi} = 0, \quad \Theta(\xi, 0) = 1, \quad \Theta(\xi, 1) = 0, \tag{3.7}$$

$$\left. \begin{aligned} f^*(\xi, 0) = \lambda\omega F(\xi, 1), \quad \eta_\delta(\xi) \frac{\partial f^*(\xi, 0)}{\partial \eta^*} = \lambda^2 \frac{\partial F(\xi, 1)}{\partial \phi}, \\ \eta_\delta^2(\xi) \frac{\partial^2 f^*(\xi, 0)}{\partial \eta^{*2}} = \lambda^3 \omega \frac{\partial^2 F(\xi, 1)}{\partial \phi^2}, \end{aligned} \right\} \tag{3.8}$$

$$\frac{\partial f^*(\xi, \infty)}{\partial \eta^*} = 1, \tag{3.9}$$

$$H_0 \left(\frac{\partial \Theta}{\partial \phi} \right)_{\phi=1} + \eta_\delta(\xi)(F)_{\phi=1} + 2\xi \eta_\delta(\xi) \left(\frac{\partial F}{\partial \xi} \right)_{\phi=1} = 0, \tag{3.10}$$

where $\omega = (\rho\mu/(\rho^*\mu^*))^{1/2}$ and $H_0 = C_p \Delta T/(P_r h_{fg})$. The form of the equations suggests a regular perturbation scheme in powers of ξ as

$$F(\xi, \phi) = \sum_{n=0}^{\infty} \xi^n F_n(\phi), \quad \Theta(\xi, \phi) = \sum_{n=0}^{\infty} \xi^n \Theta_n(\phi), \quad f^*(\xi, \eta^*) = \sum_{n=0}^{\infty} \xi^n f_n^*(\eta^*) \tag{3.11}$$

and

$$\eta_\delta(\xi) = \eta_\delta(0) + \xi \eta_\delta'(0) + \frac{\xi^2}{2} \eta_\delta''(0) + \cdots = \sum_{n=0}^{\infty} \frac{\xi^n}{n!} \frac{\mathrm{d}^n \eta_\delta}{\mathrm{d}\xi^n}(0)$$

where $\eta_\delta(\xi)$ is expressed in the form of a Taylor series expansion. The leading terms are governed by similarity equations for the problem of pure forced-convection

P_r	$\eta_\delta(0)$	$F_0''(0)$	$\Theta_0'(0)$	$Nu_x Re_x^{-1/2}$	$C_f Re_x^{1/2}$	$\delta Re_x^{1/2}/x$
1.0	0.66484	0.02460	−1.00068	1.06430	0.07870	0.94022
2.0	0.66444	0.02456	−1.00136	1.06566	0.07868	0.93966
3.0	0.66404	0.02453	−1.00204	1.06702	0.07866	0.93910
4.0	0.66364	0.02449	−1.00271	1.06838	0.07864	0.93853
5.0	0.66325	0.02446	−1.00338	1.06973	0.07863	0.93797
6.0	0.66285	0.02442	−1.00404	1.07108	0.07861	0.93741
7.0	0.66246	0.02439	−1.00471	1.07243	0.07859	0.93686
8.0	0.66206	0.02435	−1.00537	1.07377	0.07858	0.93630
9.0	0.66167	0.02432	−1.00603	1.07511	0.07856	0.93575
10.0	0.66129	0.02429	−1.00668	1.07644	0.07854	0.93520

TABLE 1. Exact numerical characteristics for various Prandtl numbers for $\xi = 0$, $H_0 = 0.008191$, $\lambda = 1$ and $\omega = 10$

H_0	$\eta_\delta(0)$	$F_0''(0)$	$\Theta_0'(0)$	$Nu_x Re_x^{-1/2}$	$C_f Re_x^{1/2}$	$\delta Re_x^{1/2}/x$
0.00002	0.1	0.00047	−1.00002	7.07121	0.06658	0.14142
0.00019	0.2	0.00191	−1.00016	3.53610	0.06736	0.28284
0.00066	0.3	0.00437	−1.00055	2.35831	0.06859	0.42426
0.00160	0.4	0.00796	−1.00133	1.77011	0.07040	0.56569
0.00325	0.5	0.01288	−1.00268	1.41801	0.07285	0.70711
0.00589	0.6	0.01937	−1.00484	1.18421	0.07609	0.84853
0.00998	0.7	0.02783	−1.00811	1.01834	0.08031	0.98995
0.01614	0.8	0.03883	−1.01292	0.89530	0.08581	1.13137
0.02545	0.9	0.05329	−1.01992	0.80133	0.09305	1.27279
0.03975	1.0	0.07265	−1.03013	0.72841	0.10275	1.41421

TABLE 2. Exact numerical characteristics for various H_0 for $\xi = 0$, $P_r = 10$, $\lambda = 1$ and $\omega = 10$

ω	$\eta_\delta(0)$	$F_0''(0)$	$\Theta_0'(0)$	$Nu_x Re_x^{-1/2}$	$C_f Re_x^{1/2}$	$\delta Re_x^{1/2}/x$
10	0.66128	0.02429	−1.00668	1.07644	0.07854	0.93519
100	1.16768	0.01375	−1.00668	0.60962	0.01427	1.65134
150	1.24507	0.01290	−1.00668	0.57172	0.01177	1.76080
500	1.38315	0.01161	−1.00668	0.51465	0.00858	1.95607
600	1.39237	0.01153	−1.00668	0.51124	0.00841	1.96911

TABLE 3. Exact numerical characteristics for various ω for $\xi = 0$, $P_r = 10$, $H_0 = 0.008191$ and $\lambda = 1$

laminar film condensation on a horizontal semi-infinite plate in a uniform stream of saturated vapour. These were first examined by Cess (1960) who assumed that the condensate flow occurs in a region of constant shear and constant heat flux. The equations were examined more fully by Beckett & Poots. On developing a thin-film approximation Cess's results were recovered. However the full similarity solutions are necessary for the detailed numerical solution which follows and the severe restrictions of the Cess analysis are not invoked.

The solutions for the leading terms at $\xi = 0$ have been obtained as special cases of the full numerical algorithm which is outlined later. Detailed results are presented in tables 1–3 for representative values of the physical parameters. The choice of $H_0 = 0.008191$ coincides with the value quoted in Koh *et al.* (1961) in their work on pure body-force-convection condensation. It is a useful comparison value in examining the successful progression of the numerical solution between known

similarity solutions. Table 1 indicates that the physical characteristics are almost independent of the Prandtl number, a common feature of condensation studies. In table 2 film thickness values $\eta_\delta(0) = 0.1(0.1)1.0$ have been specified and the associated value of H_0 identified. There is clearly a monotone relationship between increasing $\eta_\delta(0)$ and increasing H_0. Table 3 presents the results associated with variations in the shear stress parameter ω. Again the condensate film thickness increases monotonically with increasing ω but there is evidence of a large-ω asymptote. All tables indicate only slight variation in the temperature gradient $\Theta_0'(0)$. The thermal capacity effects of the condensate film are almost negligible and there is a clear justification for the common assumption of a linear temperature profile.

4. The thin film approximation near the leading edge

In the event of $\Delta T/T^* \ll 1$ or $H_0 \ll 1$ there is limited condensation from the vapour and only a thin condensate film occurs. Beckett & Poots confirm Cess's earlier suggestion that the important scale parameter is $\epsilon = H_0^{1/3}$. Series solutions in powers of ϵ can thus be developed based on the expansions

$$\left.\begin{aligned} F_0(\phi) &= \sum_{n=2}^{\infty} \epsilon^n F_{0n}(\phi), \quad \Theta_0(\phi) = \sum_{n=0}^{\infty} \epsilon^n \Theta_{0n}(\phi), \quad f_0^*(\eta^*) = \sum_{n=0}^{\infty} \epsilon^n f_{0n}^*(\eta^*), \\ \eta_\delta(0) &= \sum_{n=1}^{\infty} \epsilon^n \eta_{\delta n}(0). \end{aligned}\right\} \tag{4.1}$$

These expansions are consistent with a very small overall condensate flow rate and small free surface velocity and film thickness. Beckett & Poots have examined the first terms of these expansions and conclude that at leading order the free surface velocity is zero. Accordingly $f_{00}^*(\eta^*)$ is simply the Blasius function which possesses the well documented property

$$f_{00}^{*\prime\prime}(0) = A_0 = 0.4696. \tag{4.2}$$

The various leading terms may be readily established as

$$F_{02}(\phi) = \left(\frac{A_0}{2\lambda^3\omega}\right)^{1/3} \phi^2, \quad \Theta_{00}(\phi) = 1 - \phi, \quad \eta_{\delta 1}(0) = \left(\frac{2\lambda^3\omega}{A_0}\right)^{1/3}. \tag{4.3}$$

In contrast to the condensate velocity distribution and film thickness the vapour velocity is essentially independent of ω.

At first order in ϵ it transpires that $f_{01}^*(\eta^*) = (2/(A_0\omega^2))^{1/3} f_{00}^{*\prime}(\eta^*)$ and hence

$$f_{01}^{*\prime\prime}(0) = 0. \tag{4.4}$$

As a result

$$F_{03}(\phi) = \Theta_{01}(\phi) = \eta_{\delta 2}(0) = 0 \tag{4.5}$$

and there is no first-order contribution to the condensate flow, i.e. although there has been a non-zero tangential velocity adjustment in the first-order vapour flow it has induced no modification of the condensate flow. Only at $O(\epsilon^2)$ do adjustments for inflow of vapour at the interface modify the condensate flow.

Additionally, new higher-order energy terms may be obtained as

$$\Theta_{02}(\phi) = 0, \quad \Theta_{03}(\phi) = \frac{P_r}{12}\phi(\phi^3 - 1), \quad \Theta_{04}(\phi) = 0. \tag{4.6}$$

It is also possible to pursue further the modifications associated with the presence of gravity in the model.

The consistent forms of expansion for $F_1(\phi), \Theta_1(\phi), f_1^*(\eta^*)$ and $\eta'_\delta(0)$ are

$$\left.\begin{aligned} F_1(\phi) &= \sum_{n=3}^{\infty} \epsilon^n F_{1n}(\phi), \quad \Theta_1(\phi) = \sum_{n=4}^{\infty} \epsilon^n \Theta_{1n}(\phi), \quad f_1^*(\eta^*) = \sum_{n=2}^{\infty} \epsilon^n f_{1n}^*(\eta^*), \\ \eta'_\delta(0) &= \sum_{n=2}^{\infty} \epsilon^n \eta'_{\delta n}(0). \end{aligned}\right\} \tag{4.7}$$

After some manipulation it can be shown that

$$\left.\begin{aligned} F_{13}(\phi) &= -\frac{2\lambda^3\omega}{21A_0}\phi^2(7\phi - 9), \quad \Theta_{14}(\phi) = -\frac{P_r}{60}\left(\frac{2\lambda^3\omega}{A_0}\right)^{1/3}\phi(3\phi^4 - 5\phi^3 + 2), \\ \eta'_{\delta 2}(0) &= -\frac{2}{7}\left(\frac{2\lambda^3\omega}{A_0}\right)^{5/3} \end{aligned}\right\} \tag{4.8}$$

and flow characteristics are given by

$$\begin{aligned} Nu_x Re_x^{-1/2} &= \frac{x(\partial T/\partial y)_{y=0}}{\Delta T} Re_x^{-1/2} \\ &= \frac{1}{\sqrt{2}}\left(\frac{A_0}{2\omega H_0}\right)^{1/3}\left[1 + \frac{2\xi H_0^{1/3}}{7}\left(\frac{2\lambda^3\omega}{A_0}\right)^{4/3} + O(\xi^2 + H_0^{2/3})\right], \end{aligned} \tag{4.9}$$

$$C_f Re_x^{1/2} = \frac{\mu(\partial u/\partial y)_{y=0}}{\frac{1}{2}\rho U_\infty^2} Re_x^{1/2} = \frac{\sqrt{2}A_0}{\omega}\left[1 + \xi H_0^{1/3}\left(\frac{2\lambda^3\omega}{A_0}\right)^{4/3} + O(\xi^2 + H_0^{2/3})\right], \tag{4.10}$$

$$\delta(x) Re_x^{1/2}/x = \sqrt{2}\left(\frac{2\omega H_0}{A_0}\right)^{1/3}\left[1 - \frac{2\xi H_0^{1/3}}{7}\left(\frac{2\lambda^3\omega}{A_0}\right)^{4/3} + O(\xi^2 + H_0^{2/3})\right]. \tag{4.11}$$

These expressions are only applicable when the inflow velocity at the interface is small. For example, the deduction that $f_{00}^*(0) = 0$ becomes invalid if $\lambda\omega\epsilon^2 F_{02}(1) = O(1)$. This implies the inequality $\omega H_0 \ll (2/A_0)^{1/2} \approx 2.0637$.

As a first comparison of the above results with the exact results $\xi = 0$ is considered. The heat transfer coefficient estimate from (4.9) is shown in figure 2(*a*) compared to the results of table 2. The relative error for $\eta_\delta(0)$ up to 0.6 is less than 6%. Bearing in mind that (4.9) is a thin film estimate this is a good range of accurate correlation. The same is not true of the fixed estimate of skin friction coefficient 0.0664 from (4.10) which is 14% in error when $\eta_\delta(0) = 0.6$. In figure 3(*b*) estimates from (4.11) show only a 6% departure from exact results for the non-dimensional film thickness up to $\eta_\delta = 0.6$. The close agreement of estimates progressively deteriorates however as H_0 and ω increase. In fact the significant quantity is ωH_0 and the estimates (4.9)–(4.11) are found to be reliable for $\omega H_0 < 0.1$.

A second comparison will subsequently be drawn away from $\xi = 0$ between (4.9)–(4.11) and the exact numerical solution over all ξ.

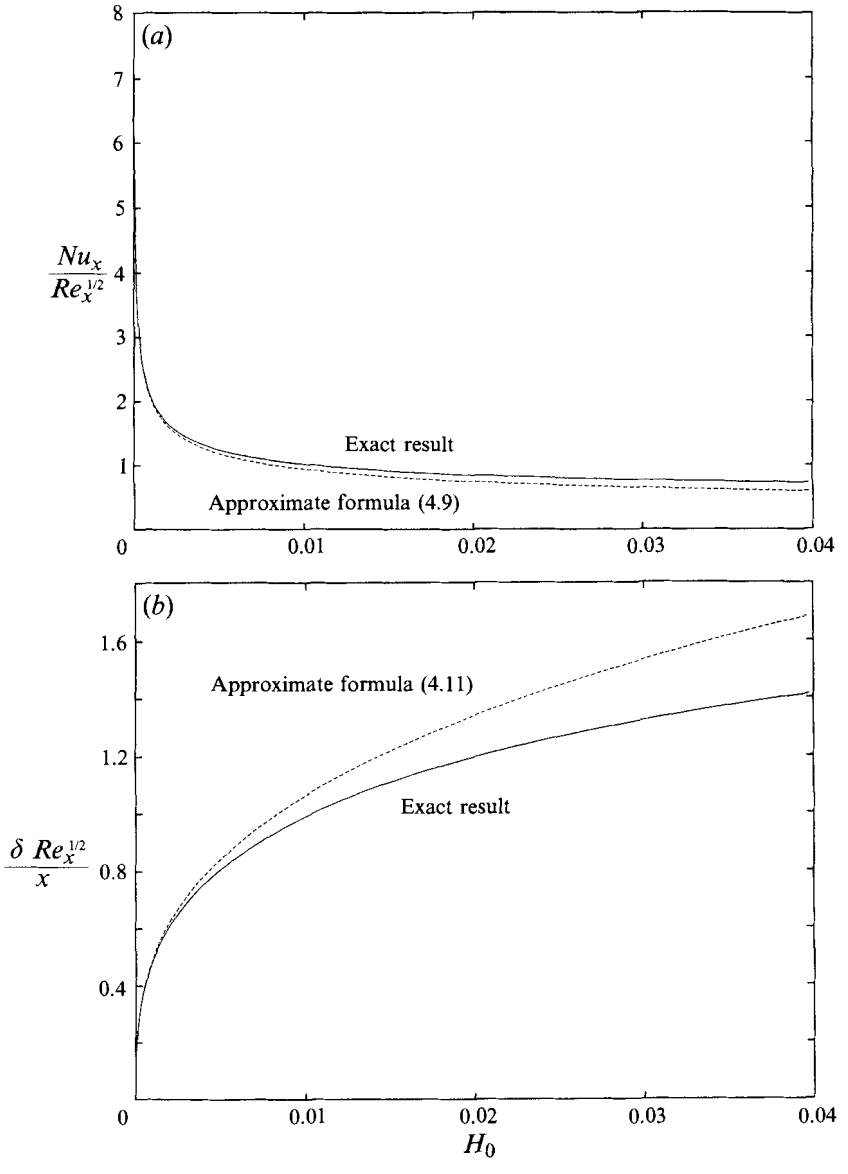

FIGURE 2. Variation of (*a*) heat transfer $Nu_x Re_x^{-1/2}$, and (*b*) condensate thickness $\delta Re_x^{1/2} x^{-1}$ with physical parameter H_0 for $\xi = 0$, $P_r = 10$, $\lambda = 1$ and $\omega = 10$.

5. The solutions for an asymptotic expansion at large ξ

Well downstream of the leading edge, gravitational acceleration of the condensate inevitably implies that the free surface velocity will overtake that of the external stream. Indeed ultimately the velocity of the free stream will be small relative to the free surface velocity. At this extreme the flow is predominantly pure body-force-convection laminar film condensation. The appropriate transformations which incorporate this progression at large ξ to an established similarity state are non-similar modifications of those of Koh *et al.* (1961). The modified transformations which again normalise the condensate thickness and, in the vapour phase, include

scalings which allow for the suction effect of condensation at the interface are

$$\psi = 4\nu\left(\frac{g(\rho-\rho^*)x^3}{4\rho\nu^2}\right)^{1/4}\bar{F}(\xi,\bar{\phi}), \qquad \bar{\phi} = \bar{\eta}/\bar{\eta}_\delta(\xi) = \frac{1}{\bar{\eta}_\delta(\xi)}\left(\frac{g(\rho-\rho^*)}{4\rho\nu^2}\right)^{1/4}\frac{y}{x^{1/4}}, \tag{5.1}$$

$$\psi^* = 4\nu\left(\frac{gx^3}{4\nu^{*2}}\right)^{1/4}\omega\bar{F}^*(\xi,\bar{\phi}^*), \qquad \bar{\phi}^* = \omega\left(\frac{g}{4\nu^{*2}}\right)^{1/4}\frac{y^*}{x^{1/4}}, \tag{5.2}$$

$$T - T^* = (T_w - T^*)\bar{\Theta}(\xi,\bar{\phi}). \tag{5.3}$$

The transformations are also consistent with the leading-order condensate flow characteristics being independent of ω, a feature of pure body-force condensation. The boundary layer equations (2.1)–(2.5) and the boundary conditions (2.6)–(2.11) transform, respectively, to the following system of equations:

$$\frac{\partial^3\bar{F}}{\partial\bar{\phi}^3} + \bar{\eta}_\delta(\xi)\left[3\bar{F}\frac{\partial^2\bar{F}}{\partial\bar{\phi}^2} - 2\left(\frac{\partial\bar{F}}{\partial\bar{\phi}}\right)^2\right] + \bar{\eta}_\delta^3(\xi) = 4\xi\left[\bar{\eta}_\delta(\xi)\frac{\partial\bar{F}}{\partial\bar{\phi}}\frac{\partial^2\bar{F}}{\partial\xi\partial\bar{\phi}} - \frac{\mathrm{d}\bar{\eta}_\delta(\xi)}{\mathrm{d}\xi}\left(\frac{\partial\bar{F}}{\partial\bar{\phi}}\right)^2 - \bar{\eta}_\delta(\xi)\frac{\partial^2\bar{F}}{\partial\bar{\phi}^2}\frac{\partial\bar{F}}{\partial\xi}\right], \qquad 0 < \bar{\phi} < 1, \tag{5.4}$$

$$\frac{1}{P_r}\frac{\partial^2\bar{\Theta}}{\partial\bar{\phi}^2} + 3\bar{\eta}_\delta(\xi)\bar{F}\frac{\partial\bar{\Theta}}{\partial\bar{\phi}} = 4\xi\bar{\eta}_\delta(\xi)\left[\frac{\partial\bar{F}}{\partial\bar{\phi}}\frac{\partial\bar{\Theta}}{\partial\xi} - \frac{\partial\bar{\Theta}}{\partial\bar{\phi}}\frac{\partial\bar{F}}{\partial\xi}\right], \qquad 0 < \bar{\phi} < 1, \tag{5.5}$$

$$\frac{\partial^3\bar{F}^*}{\partial\bar{\phi}^{*3}} + 3\bar{F}^*\frac{\partial^2\bar{F}^*}{\partial\bar{\phi}^{*2}} - 2\left(\frac{\partial\bar{F}^*}{\partial\bar{\phi}^*}\right)^2 = 4\xi\left(\frac{\partial\bar{F}^*}{\partial\bar{\phi}^*}\frac{\partial^2\bar{F}^*}{\partial\xi\partial\bar{\phi}^*} - \frac{\partial^2\bar{F}^*}{\partial\bar{\phi}^{*2}}\frac{\partial\bar{F}^*}{\partial\xi}\right), \qquad \bar{\phi}^* > 0, \tag{5.6}$$

with boundary conditions

$$\bar{F}(\xi,0) = 0, \quad \frac{\partial\bar{F}(\xi,0)}{\partial\bar{\phi}} = 0, \quad \bar{\Theta}(\xi,0) = 1, \quad \bar{\Theta}(\xi,1) = 0, \tag{5.7}$$

$$\left.\begin{aligned} &\bar{F}^*(\xi,0) = \lambda\bar{F}(\xi,1), \quad \bar{\eta}_\delta(\xi)\frac{\partial\bar{F}^*(\xi,0)}{\partial\bar{\phi}^*} = \lambda^2\omega^{-2}\frac{\partial\bar{F}(\xi,1)}{\partial\bar{\phi}}, \\ &\bar{\eta}_\delta^2(\xi)\frac{\partial^2\bar{F}^*(\xi,0)}{\partial\bar{\phi}^{*2}} = \lambda^3\omega^{-2}\frac{\partial^2\bar{F}(\xi,1)}{\partial\bar{\phi}^2}, \end{aligned}\right\} \tag{5.8}$$

$$\frac{\partial\bar{F}^*(\xi,\infty)}{\partial\bar{\phi}^*} = \tfrac{1}{2}\omega^{-2}\xi^{-1/2}, \tag{5.9}$$

$$H_0\left(\frac{\partial\bar{\Theta}}{\partial\bar{\phi}}\right)_{\bar{\phi}=1} + 3\bar{\eta}_\delta(\xi)(\bar{F})_{\bar{\phi}=1} + 4\xi\bar{\eta}_\delta(\xi)\left(\frac{\partial\bar{F}}{\partial\xi}\right)_{\bar{\phi}=1} = 0. \tag{5.10}$$

It is the form of the boundary condition (5.9) which suggests in the first instance the appropriate perturbation scheme as

$$\left.\begin{aligned} &\bar{F}(\xi,\bar{\phi}) = \bar{F}_0(\bar{\phi}) + \xi^{-1/2}\bar{F}_1(\bar{\phi}) + O(\xi^{-1}\ln\xi), \\ &\bar{\Theta}(\xi,\bar{\phi}) = \bar{\Theta}_0(\bar{\phi}) + \xi^{-1/2}\bar{\Theta}_1(\bar{\phi}) + O(\xi^{-1}\ln\xi), \\ &\bar{F}^*(\xi,\bar{\phi}^*) = \bar{F}_0^*(\bar{\phi}^*) + \xi^{-1/2}\bar{F}_1^*(\bar{\phi}^*) + O(\xi^{-1}\ln\xi), \\ &\bar{\eta}_\delta(\xi) = \bar{\eta}_\delta(\infty) + \xi^{-1/2}\bar{\eta}_\delta^*(\infty) + O(\xi^{-1}\ln\xi). \end{aligned}\right\} \tag{5.11}$$

P_r	$\bar{\eta}_\delta(\infty)$	$\bar{F}_0''(0)$	$\bar{\Theta}_0'(0)$	$\frac{Nu_x Re_x^{-1/2}}{\xi^{1/4}}$	$\frac{C_f Re_x^{1/2}}{2\xi^{3/4}}$	$\frac{\delta Re_x^{1/2}\xi^{1/4}}{x}$
1.0	0.30164	0.02721	−1.00082	2.34615	0.42289	0.42658
2.0	0.30147	0.02716	−1.00163	2.34938	0.42266	0.42634
3.0	0.30130	0.02712	−1.00245	2.35261	0.42243	0.42610
4.0	0.30113	0.02707	−1.00325	2.35582	0.42219	0.42586
5.0	0.30096	0.02703	−1.00406	2.35903	0.42197	0.42562
6.0	0.30079	0.02698	−1.00486	2.36222	0.42173	0.42539
7.0	0.30063	0.02694	−1.00565	2.36541	0.42151	0.42515
8.0	0.30046	0.02689	−1.00645	2.36858	0.42128	0.42492
9.0	0.30029	0.02685	−1.00724	2.37175	0.42106	0.42468
10.0	0.30013	0.02680	−1.00802	2.37489	0.42083	0.42445

TABLE 4. Exact numerical characteristics for various Prandtl numbers at $\xi = \infty$, $H_0 = 0.008191$, $\lambda = 1$ and $\omega = 10$

H_0	$\bar{\eta}_\delta(\infty)$	$\bar{F}_0''(0)$	$\bar{\Theta}_0'(0)$	$\frac{Nu_x Re_x^{-1/2}}{\xi^{1/4}}$	$\frac{C_f Re_x^{1/2}}{2\xi^{3/4}}$	$\frac{\delta Re_x^{1/2}\xi^{1/4}}{x}$
0.00818	0.3	0.02677	−1.00801	2.37590	0.42065	0.42426
0.02660	0.4	0.06270	−1.02489	1.81177	0.55418	0.56569
0.06920	0.5	0.11983	−1.05893	1.49756	0.67786	0.70711
0.16089	0.6	0.20022	−1.11632	1.31559	0.78653	0.84853
0.35828	0.7	0.30388	−1.20092	1.21311	0.87705	0.98995
0.80248	0.8	0.42969	−1.31327	1.16078	0.94948	1.13137
1.87632	0.9	0.57642	−1.45054	1.13965	1.00640	1.27279
4.71390	1.0	0.74337	−1.60749	1.13666	1.05128	1.41421

TABLE 5. Exact numerical characteristics for various H_0 at $\xi = \infty$, $P_r = 10$, $\lambda = 1$ and $\omega = 10$

ω	$\bar{\eta}_\delta(\infty)$	$\bar{F}_0''(0)$	$\bar{\Theta}_0'(0)$	$\frac{Nu_x Re_x^{-1/2}}{\xi^{1/4}}$	$\frac{C_f Re_x^{1/2}}{2\xi^{3/4}}$	$\frac{\delta Re_x^{1/2}\xi^{1/4}}{x}$
10	0.30013	0.02680	−1.00802	2.37489	0.42083	0.42445
100	0.29977	0.02679	−1.00802	2.37772	0.42167	0.42394
150	0.29977	0.02679	−1.00802	2.37774	0.42167	0.42394
500	0.29977	0.02679	−1.00802	2.37777	0.42168	0.42393
600	0.29977	0.02679	−1.00802	2.37777	0.42168	0.42393

TABLE 6. Exact numerical characteristics for various ω at $\xi = \infty$, $P_r = 10$, $H_0 = 0.008191$ and $\lambda = 1$

Again the leading-order terms recover the similarity solutions for body-force laminar film condensation at a vertical semi-infinite plate in surrounding quiescent vapour. In the overall numerical solution computations extended to $\xi = 10^{24}$. The extracted details assuming that similarity had been achieved at this station are presented in tables 4–6. Once again table 4 illustrates a large degree of direct independence of P_r. Of course the Prandtl number is a significant element in the definition of H_0 and herein resides its greatest influence as indicated in table 4. H_0 variations associated with $\bar{\eta}_\delta(\infty) = 0.3(0.1)1.0$ have been established. In fact the values of H_0 required to generate film thicknesses approaching unity are not realistic although they can be processed by the numerical scheme. The larger temperature gradients at these film thicknesses are therefore somewhat artificial. At realistic values of H_0 a linear

temperature profile appears to remain a useful approximation. Table 6 confirms the independence of ω of condensate characteristics.

6. Further analysis at large ξ

A feature of body-force condensation is the insensitivity, over a wide range of practical values, of the leading-order solution to ω irrespective of H_0. This feature motivates a large-parameter expansion based on $\omega \gg 1$, i.e.

$$\left.\begin{aligned} \bar{F}_0(\bar{\phi}) &= \bar{F}_{00}(\bar{\phi}) + O(\omega^{-2}), \quad \bar{\Theta}_0(\bar{\phi}) = \bar{\Theta}_{00}(\bar{\phi}) + O(\omega^{-2}), \\ \bar{F}_0^*(\bar{\phi}^*) &= \bar{F}_{00}^*(\bar{\phi}^*) + \omega^{-2}\bar{F}_{01}^*(\bar{\phi}^*) + O(\omega^{-4}), \quad \bar{\eta}_\delta(\infty) = \bar{\eta}_{\delta 0}(\infty) + O(\omega^{-2}). \end{aligned}\right\} \tag{6.1}$$

Omitting details it can be shown that the required solution in the vapour phase is simply

$$\bar{F}_{00}^*(\bar{\phi}^*) = S_0 = \text{const} \tag{6.2}$$

which represents the leading contribution to the induced suction at the condensate/vapour interface. As a result

$$\bar{F}_{01}^{*\prime}(\bar{\phi}^*) = B_0 \exp(-3S_0\bar{\phi}^*) \tag{6.3}$$

where B_0 is a further constant. In the independent limit as $H_0 \to 0$ coefficient functions may be expanded further in terms of the small parameter $H_0^{1/4}$ as

$$\left.\begin{aligned} \bar{F}_{00}(\bar{\phi}) &= H_0^{3/4}\tilde{F}_{03}(\bar{\phi}) + O(H_0), \quad \bar{\Theta}_{00}(\bar{\phi}) = \tilde{\Theta}_{00}(\bar{\phi}) + O(H_0^{1/4}), \\ \bar{\eta}_{\delta 0}(\infty) &= H_0^{1/4}\tilde{\eta}_{\delta 1}(\infty) + O(H_0^{1/2}). \end{aligned}\right\} \tag{6.4}$$

The solutions are

$$\tilde{F}_{03}(\bar{\phi}) = -\tfrac{1}{6}\bar{\phi}^2(\bar{\phi} - 3), \quad \tilde{\Theta}_{00}(\bar{\phi}) = 1 - \bar{\phi}, \quad \tilde{\eta}_{\delta 1}(\infty) = 1. \tag{6.5}$$

These are in fact the original Nusselt solutions based simply on a balance between viscous and gravitational forces on the condensate layer and a linear temperature profile.

The estimates for the vapour layer constants are then

$$S_0 = \tfrac{1}{3}\lambda H_0^{3/4}, \quad B_0 = \tfrac{1}{2}\lambda^2 H_0^{1/2}. \tag{6.6}$$

We can similarly examine the first correction terms which characterize the progression towards similarity at large ξ and consider

$$\left.\begin{aligned} \bar{F}_1(\bar{\phi}) &= \bar{F}_{10}(\bar{\phi}) + O(\omega^{-2}), \quad \bar{\Theta}_1(\bar{\phi}) = \bar{\Theta}_{10}(\bar{\phi}) + O(\omega^{-2}), \\ \bar{F}_1^*(\bar{\phi}^*) &= \bar{F}_{10}^*(\bar{\phi}^*) + \omega^{-2}\bar{F}_{11}^*(\bar{\phi}^*) + O(\omega^{-4}), \\ \bar{\eta}_\delta^*(\infty) &= \bar{\eta}_{\delta 0}^*(\infty) + O(\omega^{-2}). \end{aligned}\right\} \tag{6.7}$$

The solution for $\bar{F}_{10}^*(\bar{\phi}^*)$ is a constant S_1, the first correction to the induced suction, from which it can be established that in the vapour phase

$$\bar{F}_{11}^{*\prime}(\bar{\phi}^*) = \tfrac{1}{2} + S_1(B_1 - B_0\bar{\phi}^*)\exp(-3S_0\bar{\phi}^*). \tag{6.8}$$

Here B_1 is a further constant. This term particularly accounts for the presence of the constant velocity free stream of vapour. Again in the limit as $H_0 \to 0$ it is appropriate

to write

$$\left.\begin{aligned} \bar{F}_{10}(\bar{\phi}) = H_0^{5/4}\tilde{F}_{15}(\bar{\phi}) + O(H_0^{3/2}), \quad \bar{\Theta}_{10}(\bar{\phi}) = H_0^{3/2}\tilde{\Theta}_{16}(\bar{\phi}) + O(H_0^{7/4}), \\ \bar{\eta}^*_{\delta 0}(\infty) = H_0^{3/4}\tilde{\eta}^*_{\delta 3}(\infty) + O(H_0). \end{aligned}\right\} \tag{6.9}$$

The required solutions are

$$\left.\begin{aligned} \tilde{F}_{15}(\bar{\phi}) &= \frac{1}{16\lambda^2}\bar{\phi}^2(\bar{\phi}+1), \\ \tilde{\Theta}_{16}(\bar{\phi}) &= \frac{P_r}{480\lambda^2}\bar{\phi}(3\bar{\phi}^4 - 5\bar{\phi}^3 + 2), \\ \tilde{\eta}^*_{\delta 3}(\infty) &= -\frac{1}{8\lambda^2} \end{aligned}\right\} \tag{6.10}$$

and $S_1 = (1/8\lambda)H_0^{5/4}$, $B_1 = -(\lambda/H_0^{5/4})(4-3H_0)$. At this stage an entirely self-consistent asymptotic structure has been identified within the space of small parameters (ω^{-1}, $H_0^{1/4}, \xi^{-1/2}$) for the approach of mixed-convection laminar film condensation to the pure body-force convection limit at large ξ. Essentially this has again been arrived at in the thin-film limit $H_0 \to 0$. The contributions of the downstream perturbation have been obtained in closed form for this limit but they are extremely weak adjustments to the leading-order estimates.

The associated flow characteristics are given by

$$Nu_x Re_x^{-1/2} = \frac{\lambda}{\sqrt{2}}\left(\frac{\xi}{H_0}\right)^{1/4}[1 + O(\xi^{-1}\ln\xi + \omega^{-2} + H_0^{1/4})], \tag{6.11}$$

$$C_f Re_x^{1/2} = 2\sqrt{2}\lambda^3 H_0^{1/4}\xi^{3/4}[1 + O(\xi^{-1}\ln\xi + \omega^{-2} + H_0^{1/4})], \tag{6.12}$$

$$\delta(x) Re_x^{1/2}/x = \frac{\sqrt{2}}{\lambda}\left(\frac{H_0}{\xi}\right)^{1/4}[1 + O(\xi^{-1}\ln\xi + \omega^{-2} + H_0^{1/4})]. \tag{6.13}$$

For $H_0 \ll 1$ the initial estimates of $Nu_x Re_x^{-1/2}/\xi^{1/4}$, $C_f Re_x^{1/2}/2\xi^{3/4}$ and $\delta Re_x^{1/2}\xi^{1/4}/x$ at infinite ξ from (6.11)–(6.13) are extremely good. For example for $H_0 = 0.008191$, i.e. $H_0^{1/4} \sim 0.3$ the agreement between asymptotic estimates and exact results are within 1%, 1%, 0.4% respectively for all ω. As H_0 increases the agreement rapidly deteriorates as illustrated in figures 3(*a*)–3(*c*). However, as the full numerical solution demonstrates, the validity of estimates (6.11)–(6.13) for $H_0 \ll 1$ extends well down into the $O(1)$ range of ξ.

7. Numerical solution

Precise details in the transition range between small and large ξ can only be obtained by a full numerical solution of the governing equations (2.1)–(2.5) under boundary conditions (2.6)–(2.12). Furthermore the range of validity of asymptotic estimates can only be assessed in comparison to exact numerical solutions. In pursuing such complete numerical solutions advantage can however be taken of the clearly established limiting similarity states at small and large ξ. A continuous transformation algorithm (see Hunt & Wilks 1981) can be introduced which extracts growth rates at both extremes of ξ and ensures that integration variables remain $O(1)$ throughout the computation domain.

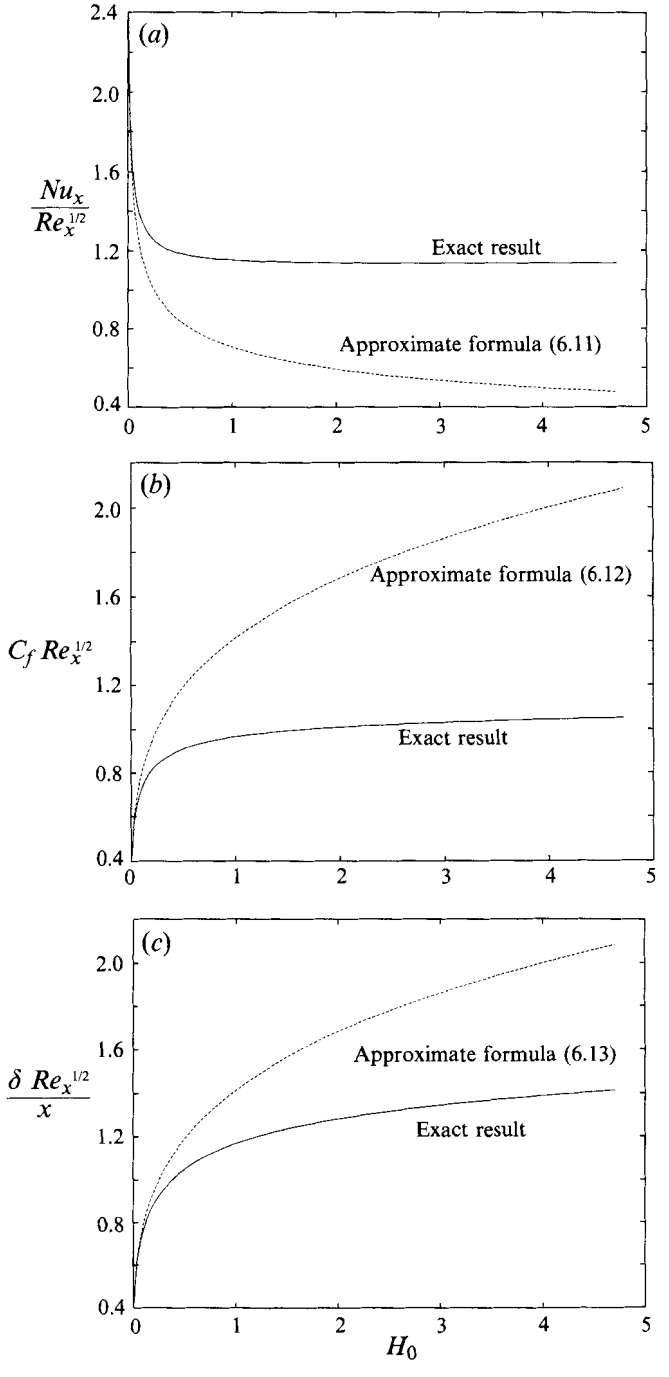

FIGURE 3. Variation of (*a*) heat transfer $Nu_x Re_x^{-1/2}$, (*b*) skin friction $C_f Re_x^{1/2}$ and (*c*) condensate thickness $\delta Re_x^{1/2} x^{-1}$ with physical parameter H_0 at $\xi = \infty$, $P_r = 10$, $\lambda = 1$ and $\omega = 10$.

ξ-dependent coefficients are introduced into transformations appropriate to the leading edge as follows:

$$\psi = \lambda(2\nu U_\infty x)^{1/2} r(\xi)\tilde{f}(\xi,\tilde{\eta}), \quad \tilde{\eta} = \lambda \frac{U_\infty^{1/2}}{2\nu^{1/2}} \frac{y}{x^{1/2}} t(\xi), \tag{7.1}$$

$$\psi^* = (2\nu^* U_\infty x)^{1/2} r^*(\xi)\tilde{f}^*(\xi,\tilde{\eta}^*), \quad \tilde{\eta}^* = \frac{U_\infty^{1/2}}{2\nu^{*1/2}} \frac{y^*}{x^{1/2}} t^*(\xi), \tag{7.2}$$

$$T - T^* = (T_w - T^*)s(\xi)\tilde{\theta}(\xi,\tilde{\eta}). \tag{7.3}$$

The objective is to establish functions $r(\xi), t(\xi), r^*(\xi), t^*(\xi)$ and $s(\xi)$ which effect a smooth transition from the leading-edge similarity regime to the downstream similarity state. Without loss of generality one can prescribe

$$r(0) = s(0) = t(0) = r^*(0) = t^*(0) = 1.$$

Examining the correlations between leading-edge and downstream transformations leads to

$$\left.\begin{aligned} r(\xi) = (1+16\xi)^{1/4}, \quad s(\xi) = 1, \quad t(\xi) = (1+\xi)^{1/4}, \\ r^*(\xi) = (1+16\xi)^{1/4}, \quad t^*(\xi) = (1+\xi)^{1/4}. \end{aligned}\right\} \tag{7.4}$$

The resulting unified basis of computation is now the system of equations

$$\frac{\partial^3\tilde{f}}{\partial\tilde{\eta}^3} + \frac{1+24\xi}{(1+\xi)^{1/4}(1+16\xi)^{3/4}}\tilde{f}\frac{\partial^2\tilde{f}}{\partial\tilde{\eta}^2} - \frac{\xi(17+32\xi)}{2(1+\xi)^{5/4}(1+16\xi)^{3/4}}\left(\frac{\partial\tilde{f}}{\partial\tilde{\eta}}\right)^2 + \frac{2\xi}{(1+\xi)^{3/4}(1+16\xi)^{1/4}} + \frac{2\xi(1+16\xi)^{1/4}}{(1+\xi)^{1/4}}\left\{\frac{\partial\tilde{f}}{\partial\xi}\frac{\partial^2\tilde{f}}{\partial\tilde{\eta}^2} - \frac{\partial\tilde{f}}{\partial\tilde{\eta}}\frac{\partial^2\tilde{f}}{\partial\xi\partial\tilde{\eta}}\right\} = 0, \tag{7.5}$$

$$\frac{\partial^2\tilde{\theta}}{\partial\tilde{\eta}^2} + P_r\left[\frac{1+24\xi}{(1+\xi)^{1/4}(1+16\xi)^{3/4}}\tilde{f}\frac{\partial\tilde{\theta}}{\partial\tilde{\eta}} + 2\xi\frac{(1+16\xi)^{1/4}}{(1+\xi)^{1/4}}\left\{\frac{\partial\tilde{f}}{\partial\xi}\frac{\partial\tilde{\theta}}{\partial\tilde{\eta}} - \frac{\partial\tilde{f}}{\partial\tilde{\eta}}\frac{\partial\tilde{\theta}}{\partial\xi}\right\}\right] = 0, \tag{7.6}$$

$$\frac{\partial^3\tilde{f}^*}{\partial\tilde{\eta}^{*3}} + \frac{1+24\xi}{(1+\xi)^{1/4}(1+16\xi)^{3/4}}\tilde{f}^*\frac{\partial^2\tilde{f}^*}{\partial\tilde{\eta}^{*2}} - \frac{\xi(17+32\xi)}{2(1+\xi)^{5/4}(1+16\xi)^{3/4}}\left(\frac{\partial\tilde{f}^*}{\partial\tilde{\eta}^*}\right)^2 + \frac{2\xi(1+16\xi)^{1/4}}{(1+\xi)^{1/4}}\left\{\frac{\partial\tilde{f}^*}{\partial\xi}\frac{\partial^2\tilde{f}^*}{\partial\tilde{\eta}^{*2}} - \frac{\partial\tilde{f}^*}{\partial\tilde{\eta}^*}\frac{\partial^2\tilde{f}^*}{\partial\xi\partial\tilde{\eta}^*}\right\} = 0, \tag{7.7}$$

$$H_0\left[\left(\frac{\partial\tilde{\theta}}{\partial\tilde{\eta}}\right)_{\tilde{\eta}=0} + P_r\frac{1+24\xi}{(1+\xi)^{1/4}(1+16\xi)^{3/4}}\int_0^{\tilde{\eta}_\delta(\xi)}\frac{\partial\tilde{f}}{\partial\tilde{\eta}}\tilde{\theta}\,\mathrm{d}\tilde{\eta} + 2\xi P_r\frac{(1+16\xi)^{1/4}}{(1+\xi)^{1/4}}\int_0^{\tilde{\eta}_\delta(\xi)}\left(\frac{\partial^2\tilde{f}}{\partial\xi\partial\tilde{\eta}}\tilde{\theta} + \frac{\partial\tilde{f}}{\partial\tilde{\eta}}\frac{\partial\tilde{\theta}}{\partial\xi}\right)\mathrm{d}\tilde{\eta}\right] + \frac{1+24\xi}{(1+\xi)^{1/4}(1+16\xi)^{3/4}}(\tilde{f})_{\tilde{\eta}=\tilde{\eta}_\delta(\xi)} + 2\xi\frac{(1+16\xi)^{1/4}}{(1+\xi)^{1/4}}\left(\frac{\partial\tilde{f}}{\partial\xi}\right)_{\tilde{\eta}=\tilde{\eta}_\delta(\xi)} + 2\xi\frac{(1+16\xi)^{1/4}}{(1+\xi)^{1/4}}\left(\frac{\partial\tilde{f}}{\partial\tilde{\eta}}\right)_{\tilde{\eta}=\tilde{\eta}_\delta(\xi)}\frac{\mathrm{d}\tilde{\eta}_\delta(\xi)}{\mathrm{d}\xi} = 0. \tag{7.8}$$

where in the $(\xi,\tilde{\eta})$-plane the thickness of the condensate layer is $\tilde{\eta}_\delta(\xi)$. The boundary conditions read

$$\tilde{f}(\xi,0) = 0, \quad \frac{\partial\tilde{f}(\xi,0)}{\partial\tilde{\eta}} = 0, \quad \tilde{\theta}(\xi,0) = 1, \quad \tilde{\theta}(\xi,\tilde{\eta}_\delta(\xi)) = 0, \tag{7.9}$$

$$\left.\begin{aligned} \tilde{f}^*(\xi,0) = \lambda\omega\tilde{f}(\xi,\tilde{\eta}_\delta(\xi)), \quad \frac{\partial\tilde{f}^*(\xi,0)}{\partial\tilde{\eta}^*} = \lambda^2\frac{\partial\tilde{f}(\xi,\tilde{\eta}_\delta(\xi))}{\partial\tilde{\eta}}, \\ \frac{\partial^2\tilde{f}^*(\xi,0)}{\partial\tilde{\eta}^{*2}} = \lambda^3\omega\frac{\partial^2\tilde{f}(\xi,\tilde{\eta}_\delta(\xi))}{\partial\tilde{\eta}^2}, \end{aligned}\right\} \tag{7.10}$$

$$\frac{\partial\tilde{f}^*(\xi,\infty)}{\partial\tilde{\eta}^*} = \frac{1}{(1+\xi)^{1/4}(1+16\xi)^{1/4}}. \tag{7.11}$$

Accordingly the formulas for the flow characteristics are

$$Nu_x Re_x^{-1/2} = -\frac{\lambda}{\sqrt{2}}s(\xi)t(\xi)\tilde{\theta}_{\tilde{\eta}}(\xi,0) = -\frac{\lambda}{\sqrt{2}}(1+\xi)^{1/4}\tilde{\theta}_{\tilde{\eta}}(\xi,0), \tag{7.12}$$

$$C_f Re_x^{1/2} = \sqrt{2}\lambda^3 r(\xi)t^2(\xi)\tilde{f}_{\tilde{\eta}\tilde{\eta}}(\xi,0) = \sqrt{2}\lambda^3(1+16\xi)^{1/4}(1+\xi)^{1/2}\tilde{f}_{\tilde{\eta}\tilde{\eta}}(\xi,0). \tag{7.13}$$

Finally the condensate thickness yields

$$\frac{\delta(x)Re_x^{1/2}}{x} = \frac{\sqrt{2}}{\lambda t(\xi)}\tilde{\eta}_\delta(\xi) = \frac{\sqrt{2}}{\lambda(1+\xi)^{1/4}}\tilde{\eta}_\delta(\xi). \tag{7.14}$$

Numerical solutions of the limiting similarity states have previously been achieved by separate integration of the condensate and vapour phase equations coupled only by an iterative guessing strategy designed to accommodate conditions at the interface. The non-similarity of the present problem and the inherent ξ-dependence along the plate motivate against this strategy. Moreover it has been common to specify the condensate thickness and subsequently identify the associated value of H_0. Here $\tilde{\eta}_\delta(\xi)$ is an evolving element of the solution and it is necessary to prescribe the H_0 common to the whole flow field as evaluated in a given physical configuration of temperature differential and associated fluid properties.

With these points in mind a new method of solution has been developed which is appropriate to quite general systems of differentio-integral equations describing multilayer, multiphase and interface situations. The method is comprehensively reported in a companion paper by Shu & Wilks (1995). The method incorporates a combination of merging and reduction procedures. Unitary functions common to both phases are defined over an extension of the normalized condensate layer $0 < \phi = \tilde{\eta}/\tilde{\eta}_\delta(\xi) < \infty$ and by utilizing the Heaviside step function a single momentum and a single energy equation can be obtained. Variables at the interface are regarded as multi-valued with left- and right-hand limiting values accommodating the interfacial conditions. Simultaneously the integral balance of mass condensation flow is reduced to a discrete model representation involving the unitary functions.

The parabolic system is then solved using a marching technique which obtains a solution at ξ_{n+1} on the basis of a valid known solution at ξ_n. The method used is an adaptation of the Keller box method (Keller & Cebeci 1971) which is adjusted to deal with the finite condensate film thickness and the mass flow driven by the phase change. The equations are written as a set of first-order equations and an arbitrary rectangular net of points is placed over $\xi \leqslant 0, 0 \leqslant \phi \leqslant \phi_\infty$ with the only restriction that the point $\phi = 1$ must be included as a mesh point. As a consequence $\tilde{\eta}_\delta(\xi)$ appears directly as one of the unknowns. Outline details of the solution algorithm are given in the Appendix.

Since central differences are used the exact numerical solution of the difference equations is a second-order-accurate approximation with respect to the chosen rect-

angular net of points

$$\xi_0 = 0, \quad \xi_n = \xi_{n-1} + k_n, \qquad n = 1, 2, \cdots;$$
$$\phi_0 = 0, \quad \phi_j = \phi_{j-1} + h_j, \qquad j = 1, 2, \cdots, J_1, \cdots, J_2;$$

where $\phi_{J_1} = 1$ and $\phi_{J_2} = \phi_\infty$.

The local truncation errors of the difference scheme can thus be written as a Taylor series in powers of h^2 and k^2 where $k = \max_n k_n$ and $h = \max_j h_j$. It is therefore possible, by solving the problem on different sized grids and using Richardson's extrapolation, to produce results of high accuracy provided the truncation errors are larger than the iteration errors. Here each cell of the net has been divided into m subintervals both in the ξ-direction and in the ϕ-direction, where m is an integer. The problem has then been solved numerically for $m = 1, 2, 3$ and 4 to produce results of $O(k^8 + h^8)$ accuracy.

8. Results and comparisons

It has already been demonstrated that the numerical solution reproduces with high accuracy the flow characteristics of the limiting similarity states. The solutions at these extremes have indicated the limitations of the thin-film asymptotes associated with $H_0^{1/3}$ and $H_0^{1/4}$ as ωH_0 increases. To illustrate the solution over all ξ a particular set of parameters has been specified which is known to generate a moderate-to-thin film thickness throughout the flow field. The choice of parameters coincides with a particular case examined in Koh *et al.* (1961) for which a pure body-force solution was obtained based upon a film thickness of $\tilde{\eta}_\delta = 0.3$. Together with values $\lambda = 1, P_r = 10$ and $\omega = 10$ the coupled solution obtained unknown interfacial boundary conditions which led to an estimate $H_0 = 0.008191$. In contrast a detailed numerical solution was obtained here for the overall problem with $H_0 = 0.008191$ specified and the film thickness allowed to progress within the solution to its downstream asymptote. The results are presented in table 7. In view of the extrapolation procedures the downstream film thickness $\tilde{\eta}_\delta(\infty) = 0.30013$ is thought to be a more accurate estimate for this H_0. Nevertheless the results of this numerical computation are taken as confirmation of the viability of the numerical scheme and its successful implementation. This set of parameters has also been used as the basis for comparison between upstream and downstream thin-film asymptotes although the initial film thickness $\tilde{\eta}_\delta = 0.66219$ may be thought of as moderate. Indeed this is apparent in figure 4(*a*) where the non-dimensional condensate thickness is plotted over all ξ and is compared with the thin film asymptotes. At $\xi = 0$ the thin film estimate is in error by 6.5%. The thin-film gravity correction term provides a reasonable estimate up to $\xi \sim 2 \times 10^{-2}$. In contrast at large ξ there is less than 1% discrepancy between exact and approximate results. The asymptotic estimate remains in error by less than 2% as far as $\xi = 0$. Further comparisons are drawn in figures 4(*b*) and 4(*c*) between exact results and asymptotic estimates for both the heat transfer coefficient and the skin friction coefficient. Again discrepancies at $\xi = 0$ reflect the evaluation of a thin film estimate in a moderate-film context. Nevertheless the gravity correction term improves the range of valid estimates and the downstream asymptotes have a range of utility as far as ξ of $O(1)$. Notice that $\omega H_0 \sim 0.1$ for these computations, which is approaching the limit of validity of the thin-film approximations.

Earlier the possible existence of a large-ω asymptote for characteristics at the plate was hinted at. In figure 5 there is evidence that such an asymptote prevails throughout

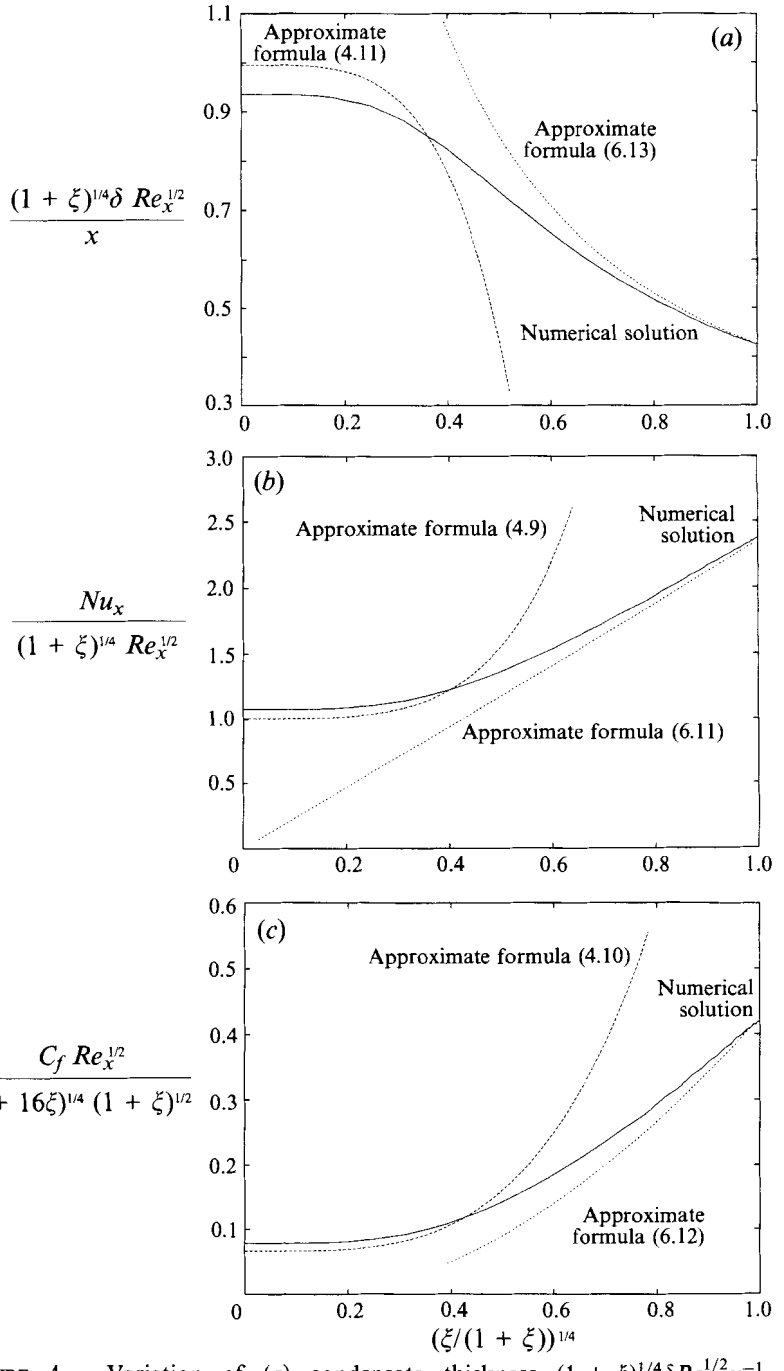

FIGURE 4. Variation of (*a*) condensate thickness $(1+\xi)^{1/4}\delta Re_x^{1/2}x^{-1}$, (*b*) heat transfer $Nu_x(1+\xi)^{-1/4}Re_x^{-1/2}$ and (*c*) skin friction $C_f Re_x^{1/2}(1+16\xi)^{-1/4}(1+\xi)^{-1/2}$ for $P_r = 10$, $H_0 = 0.008191$, $\lambda = 1$ and $\omega = 10$.

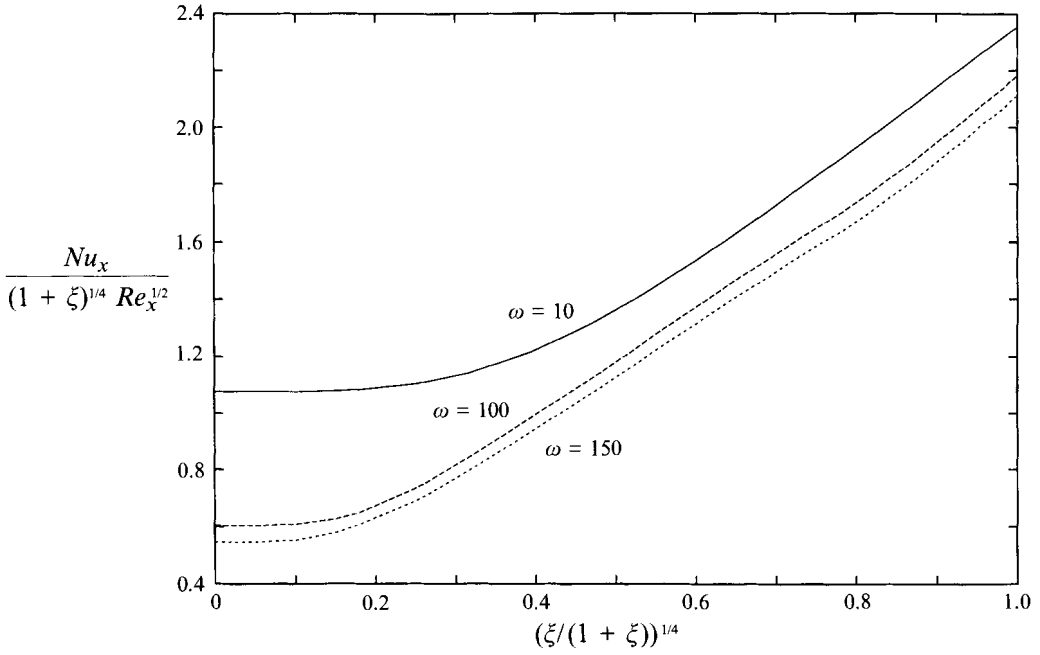

FIGURE 5. Variation of heat transfer $Nu_x(1+\xi)^{-1/4}Re_x^{-1/2}$ with $\rho\mu$ ratio ω for $P_r = 1$, $H_0 = 0.008191$ and $\lambda = 1$.

ξ	$\tilde{\eta}_\delta(\xi)$	$\tilde{f}_{\tilde{\eta}\tilde{\eta}}(\xi, \tilde{\eta}_\delta(\xi))$	$\frac{Nu_x Re_x^{-1/2}}{(1+\xi)^{1/4}}$	$\frac{C_f Re_x^{1/2}}{(1+16\xi)^{1/4}(1+\xi)^{1/2}}$	$\frac{(1+\xi)^{1/4}\delta Re_x^{1/2}}{x}$
0.0	0.66129	0.02422	1.07644	0.07854	0.93520
0.2	0.44109	0.00730	1.61486	0.20417	0.62379
1.0	0.35121	0.00268	2.02617	0.31715	0.49668
2.0	0.32859	0.00164	2.16741	0.35995	0.46470
5.0	0.31239	0.00084	2.27979	0.39428	0.44179
10.0	0.30635	0.00048	2.32471	0.40772	0.43325
30.0	0.30239	0.00016	2.35226	0.41480	0.42765
60.0	0.30118	0.00004	2.36458	0.41859	0.42593
100	0.30094	−0.00001	2.36353	0.41747	0.42560
10^4	0.30045	−0.00017	2.37021	0.41901	0.42490
10^{24}	0.30013	−0.00019	2.37489	0.42083	0.42445

TABLE 7. Exact numerical characteristics over ξ for $P_r = 10$, $H_0 = 0.008191$, $\lambda = 1$ and $\omega = 10$

the whole flow field. Heat transfer coefficients have been plotted for $\omega = 10, 100, 150$. The numerical results appear sensitive only to low values of ω. Fujii & Uehara (1972) quote typical values of ω for water and a variety of organic substances as $O(10^2)$ and above. For practical purposes estimates of heat transfer coefficients based on a single large value of ω may suffice.

A particularly useful comparison can be made with the approximate solution of Fujii & Uehara (1972) which is essentially a thin-film approximation obtained by momentum integral techniques. These authors quote the following estimate for the heat transfer coefficient:

ξ	$Nu_x Re_x^{-1/2}$	
	Shu & Wilks Exact	Fujii & Uehara Equation (8.1)
0.0	1.07644	1.06907
0.2	1.69017	1.64992
1.0	2.40954	2.37520
2.0	2.85247	2.81001
5.0	3.56806	3.52224
10.0	4.23367	4.18422
30.0	5.55042	5.50283
60.0	6.60825	6.54284
100	7.49275	7.43357
10^4	2.37027×10^1	2.35045×10^1
10^{24}	2.37489×10^6	2.35045×10^6

TABLE 8. Heat transfer coefficient comparison between exact results and approximate correlation (8.1) for $P_r = 10$, $H_0 = 0.008191$, $\lambda = 1$ and $\omega = 10$

ωH_0	$Nu_x Re_x^{-1/2}$			
	Shu & Wilks		Fujii & Uehara	
	$\xi = 0$	$\xi = 10^4$	$\xi = 0$	$\xi = 10^4$
0.5	0.698	0.159×10^2	0.663	0.150×10^2
1.0	0.630	0.141×10^2	0.585	0.126×10^2
2.0	0.596	0.128×10^2	0.537	0.106×10^2
5.0	0.586	0.119×10^2	0.503	0.084×10^2

TABLE 9. Comparison of $Nu_x Re_x^{-1/2}$ from exact results and the correlation of Fujii & Uehara (8.1) for $P_r = 10$, $\lambda = 1$ and $\omega = 10$

$$Nu_x Re_x^{-1/2} = K(\omega H_0)\left(1 + \frac{1}{4K^4(\omega H_0)}\frac{\xi}{H_0}\right)^{1/4}, \tag{8.1}$$

where $K = 0.450(1.20 + 1/\omega H_0)^{1/3}$.

In the first instance in table 8 we compare this estimate with the exact numerical solution table 7. The agreement is remarkably good over all ξ. This may be ascribed to the value $\omega H_0 = 0.08191$ being within the range of validity of the thin-film approximation. A more stringent test can be made by drawing comparisons with increasing ωH_0. The results are presented in table 9. There is a noticeable deterioration as compared with the full numerical solution.

Finally in figure 6 comparisons are made between Jacobs' experimental results using Freon 113 and exact numerical solutions. Notwithstanding the experimental difficulties and the scatter associated with air in the vapour flow there is a high degree of correlation between the overall features and the exact solutions. Here $\omega H_0 = 0.617, 2.468$ and 4.319 with $\omega = 100$ have been used for comparison as the nearest estimates to the parameters quoted by Jacobs in a slightly different form.

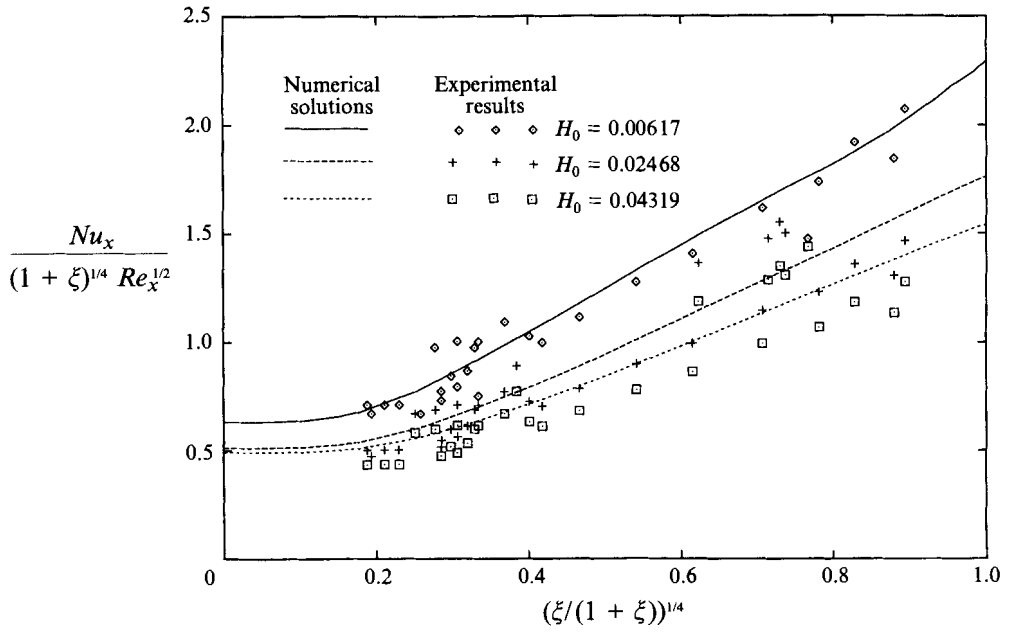

FIGURE 6. Comparison of numerical and experimental results of heat transfer $Nu_x(1+\xi)^{-1/4}Re_x^{-1/2}$ for various physical parameter H_0 at $P_r = 1$, $\lambda = 1$ and $\omega = 100$ for Freon 113.

9. Conclusions

Detailed asymptotic analyses of the perturbed limiting similarity states associated with mixed-convection laminar film condensation flow over a semi-infinite vertical plate have been developed. Additionally a formulation of the problem incorporating the intrinsic physical features at the respective limits of pure forced and pure body-force condensation has been presented. The formulation has been shown to provide a convenient framework for a comprehensive numerical solution. Numerical solutions have been established using a new technique based upon modification of the Keller-box scheme. An entirely satisfactory synthesis between thin-film asymptotic and numerical results has been demonstrated although over a significant transitional range of ξ flow characteristics can only be precisely estimated by the numerical solution. Comparisons with experiment in this transitional range have provided valuable mutual corroboration of the model and solution scheme. In particular we have been able to examine the value of a previously reported thin-film approximation to the heat transfer coefficient as ωH_0 increases and the thin-film hypothesis is no longer strictly valid.

The work presented provides the basis for further examination of a wider range of configurations which include multilayer, interfacial and multiphase features.

Appendix. The numerical algorithm

With respect to the net of points

$$\xi_0 = 0, \quad \xi_n = \xi_{n-1} + k_n, \qquad n = 1, 2, \cdots;$$
$$\phi_0 = 0, \quad \phi_j = \phi_{j-1} + h_j, \qquad j = 1, 2, \cdots, J_1, \cdots, J_2;$$

over $\xi \geqslant 0$, $0 \leqslant \phi \leqslant \phi_\infty$, where $\phi_{J_1} = 1$ and $\phi_{J_2} = \phi_\infty$, the discretized system of equations reduces to $5J_2 + 11$ nonlinear equations for $5J_2 + 11$ unknown dependents including specifically $\tilde{\eta}_\delta(\xi)$. Newton's method is used to obtain linear equations for the increments between the i and $i+1$ iterates. The resulting linear system of algebraic equations is supplemented by four additional dummy variables to yield a $5J_2 + 15$ system of equations

$$\boldsymbol{A}^{(i)}\vec{\Delta}^{(i)} = \boldsymbol{q}^{(i)} \qquad i = 0, 1, 2, \cdots\cdots \tag{A 1}$$

where $\vec{\Delta}^{(i)}$ is the column vector of Newton increments and $\boldsymbol{q}^{(i)}$ is a known column vector. The algorithm is characterized by a block arrow-like coefficient matrix

$$\boldsymbol{A}^{(i)} = \begin{pmatrix} \boldsymbol{A}_0 & \boldsymbol{C}_0 & & & & & & & \boldsymbol{D}_0 \\ \boldsymbol{B}_1 & \boldsymbol{A}_1 & \boldsymbol{C}_1 & & & & & & \boldsymbol{D}_1 \\ & \boldsymbol{B}_2 & \boldsymbol{A}_2 & \boldsymbol{C}_2 & & & & & \boldsymbol{D}_2 \\ & & \cdot & \cdot & \cdot & & & & \cdot \\ & & & \cdot & \cdot & \cdot & & & \cdot \\ & & & & \cdot & \cdot & \cdot & & \cdot \\ & & & & & \boldsymbol{B}_{N-1} & \boldsymbol{A}_{N-1} & \boldsymbol{C}_{N-1} & \boldsymbol{D}_{N-1} \\ & & & & & & \boldsymbol{B}_N & \boldsymbol{A}_N & \boldsymbol{D}_N \\ \boldsymbol{E}_0 & \boldsymbol{E}_1 & \boldsymbol{E}_2 & \cdot & \cdot & \cdot & \boldsymbol{E}_{N-1} & \boldsymbol{E}_N & \boldsymbol{A}_{N+1} \end{pmatrix}$$

where individual matrices are of order 5 and $N = J_2 + 1$. Using an appropriate factorization $\boldsymbol{A}^{(i)} = \boldsymbol{L}\boldsymbol{U}$ the system (A 1) can be reduced to the equivalent system

$$\boldsymbol{L}\boldsymbol{z}^{(i)} = \boldsymbol{q}^{(i)}, \quad \boldsymbol{U}\vec{\Delta}^{(i)} = \boldsymbol{z}^{(i)}, \qquad i = 0, 1, 2, \cdots\cdots. \tag{A 2}$$

The intermediate vectors $z_j^{(i)}$ are 5-component column vectors which are instrumental in establishing the final algorithm for solving the matrix equation as

$$\left.\begin{aligned} &\boldsymbol{Q} \longleftarrow \boldsymbol{A}_0^{-1}, \quad \boldsymbol{q}_0^{(i)} \longleftarrow \boldsymbol{Q}\boldsymbol{q}_0^{(i)}, \quad \boldsymbol{D}_0 \longleftarrow \boldsymbol{Q}\boldsymbol{D}_0, \\ &\left.\begin{aligned} &\boldsymbol{A}_{j-1} \longleftarrow \boldsymbol{Q}\boldsymbol{C}_{j-1}, \qquad \boldsymbol{E}_j \longleftarrow \boldsymbol{E}_j - \boldsymbol{E}_{j-1}\boldsymbol{A}_{j-1} \\ &\qquad\qquad\qquad\quad \boldsymbol{Q} \longleftarrow (\boldsymbol{A}_j - \boldsymbol{B}_j\boldsymbol{A}_{j-1})^{-1} \\ &\boldsymbol{q}_j^{(i)} \longleftarrow \boldsymbol{Q}(\boldsymbol{q}_j^{(i)} - \boldsymbol{B}_j\boldsymbol{q}_{j-1}^{(i)}), \quad \boldsymbol{D}_j \longleftarrow \boldsymbol{Q}(\boldsymbol{D}_j - \boldsymbol{B}_j\boldsymbol{D}_{j-1}) \end{aligned}\right\}, j = 1, 2, \cdots, J_2 + 1, \\ &\boldsymbol{Q} \longleftarrow (\boldsymbol{A}_{J_2+2} - \sum_{k=0}^{J_2+1} \boldsymbol{E}_k\boldsymbol{D}_k)^{-1}, \\ &\vec{\Delta}_{J_2+2}^{(i)} \longleftarrow \boldsymbol{Q}(\boldsymbol{q}_{J_2+2}^{(i)} - \sum_{k=0}^{J_2+1} \boldsymbol{E}_k\boldsymbol{q}_k^{(i)}), \\ &\vec{\Delta}_{J_2+1}^{(i)} \longleftarrow \boldsymbol{q}_{J_2+1}^{(i)} - \boldsymbol{D}_{J_2+1}\vec{\Delta}_{J_2+2}^{(i)}, \\ &\vec{\Delta}_j^{(i)} \longleftarrow \boldsymbol{q}_j^{(i)} - \boldsymbol{A}_j\vec{\Delta}_{j+1}^{(i)} - \boldsymbol{D}_j\vec{\Delta}_{J_2+2}^{(i)}, \quad j = J_2, J_2 - 1, \cdots, 0, \end{aligned}\right\} \tag{A 3}$$

where $\longleftarrow$ denotes replacement. Algorithmically this is a modification of the usual solution of a block tridiagonal system to include the $\boldsymbol{D}_j$ and $\boldsymbol{E}_j$. The algorithm can be made efficient by taking account of the zeros appearing in matrices.

REFERENCES

BECKETT, P. & POOTS, G. 1972 Laminar film condensation in forced flows. *Q. J. Mech. Appl. Maths* **25**, 125–152.

CESS, R. D. 1960 Laminar-film condensation on a flat plate in the absence of a body force. *Z. Angew. Math. Phys.* **11**, 426–433.

CHUNG, P. M. 1961 Film condensation with and without body force in boundary layer flow of vapor over a flat plate. *NASA Tech. Note* D-790.

FUJII, T. & UEHARA, H. 1972 Laminar filmwise condensation on a vertical surface. *Intl J. Heat Mass Transfer* **15**, 217–233.

HARTREE, D. R. & WOMERSLEY, J. R. 1937 A method for the numerical or mechanical solution of certain types of partial differential equations. *Proc. R. Soc. Lond.* A **161**, 353–366.

HUNT, R. & WILKS, G. 1981 Continuous transformation computation of boundary layer equations between similarity regimes. *J. Comput. Phys.* **40**, 478–490.

JACOBS, H. R. 1965 Combined body force with forced convection in laminar film condensation heat transfer of Freon 113. PhD thesis, Department of Mechanical Engineering, Ohio State University.

JACOBS, H. R. 1966 An integral treatment of combined body force and forced convection in laminar film condensation. *Intl J. Heat Mass Transfer* **9**, 637–648.

KELLER, H. B. & CEBECI, T. 1971 Accurate numerical methods for boundary layer flows. I: two dimensional laminar flows. *Proc. 2nd Intl Conf. on Numerical Methods in Fluid Dynamics, Berkeley, California*, pp. 92–100.

KOH, J. C. Y. 1962 Film condensation in a forced-convection boundary-layer flow. *Intl J. Heat Mass Transfer* **5**, 941–954.

KOH, J. C. Y., SPARROW E. M. & HARTNETT, J. P. 1961 The two phase boundary layer in laminar film condensation. *Intl J. Heat Mass Transfer* **2**, 69–82.

NUSSELT, W. 1916 Die Oberflächen-Kondensation des Wasserdampfes. *Z. Verein. Deutsch. Ing.* **60**, 541–569 (in German).

RAJU, M. S., LIU, X. Q. & LAW, C. K. 1984 A formulation of combined forced and free convection past horizontal and vertical surfaces. *Intl J. Heat Mass Transfer* **27**, 2215–2224.

ROHSENOW, W. M. 1956 Heat transfer and temperature distribution in laminar-film condensation. *Trans. ASME* **78**, 1645–1648.

SHU, J.-J. & WILKS, G. 1995 An accurate numerical method for systems of differentio-integral equations associated with multiphase flow. *Computers Fluids* (to appear).

SPARROW, E. M. & GREGG, J. L. 1959 A boundary-layer treatment of laminar-film condensation. *Trans. ASME* C: *J. Heat Transfer* **81**, 13–18.

TERRILL, R. M. 1960 Laminar boundary-layer flow near separation with and without suction. *Phil. Trans. R. Soc. Lond.* A **253**, 55–100.